EXPERIMENTAL STUDIES ON THE TAYLOR-COUETTE FLOW OF SHEAR-THINNING FLUIDS

*Tatsuya Kawaguchi, Yuki Tano and Takushi Saito

Tokyo Institute of Technology, Japan

ABSTRACT: Two concentric cylinders with the inner cylinder rotating cause circumferential flow with a Taylor vortex under a certain range of Reynolds numbers. This is called Taylor–Couette flow. It has been the focus of extensive study in terms of Newtonian fluids but not non-Newtonian fluids. Despite various industrial applications, the flow transition mechanism of the flow remains unclear. Therefore, many kinds of apparatuses using Taylor–Couette flow in the redesign and scale-up are still under investigation. The objective of the present study is first to determine the transition points of Taylor-vortex flow and the wavy vortex flow regime with a non-Newtonian working fluid. To understand the effect of the working fluid, two kinds of shear-thinning liquids with different structural viscosity indices were compared. Particle image velocimetry (PIV) was used as the flow visualization technique for a wide range of Reynolds numbers. A water solution of guar gum resulted in a stable six-cell mode in the Taylor-vortex flow and wavy-vortex flow regimes. The other working fluid, with xanthan gum, resulted in a vertically enlarged oval vortex that appeared under the same Reynolds number range. Both results were significantly different from the flow with Newtonian working fluid. In conclusion, we confirm that the shear-thinning characteristics of the working fluid affect the aspect ratio of the edge vortex as well as the drifting of the vortex center along the axis of the cylinder.

Keywords: Non-Newtonian Fluids, Taylor Vortex Flow, Wavy Vortex Flow, Shear-thinning, Particle Image Velocimetry

1. INTRODUCTION

Two concentric cylinders in which one or both are rotating result in circumferential flow with a Taylor vortex at certain Reynolds numbers. This is called Taylor–Couette flow. Taylor–Couette flow has been applied in various industries, including the food processing, chemical reactors, and medical fabrication industries. It has been used to improve in many industrial applications, such as filtration [1], protein shearing [2], blood detoxification [3], liquid–liquid extraction [4], bioreactors [5], emulsion polymerization [6], crystallization [7], cultivation of animal cells [5] and photocatalytic reactions [8]. Moreover, many industrial applications of the aforementioned flow within double concentric cylinders operate with non-Newtonian working fluids. From the point of view of complex fluid analysis, Ashrafi [9] pointed out that Taylor–Couette flow with non-Newtonian working fluids plays an important role in the rheology of flow instabilities. As mentioned, there are many case studies on complex fluids, and many kinds of apparatuses using Taylor–Couette flow of redesign and scale up are still under investigation. Many applications of Taylor–Couette flow employ shear-thinning fluids, and some researchers [9-12] have pointed out that detailed experimental investigations on shear-thinning fluids are lacking. Against this background, the objective of the present research is to determine the flow transition

mechanism of flow in a concentric rotating cylinder with non-Newtonian working fluids.

Theory for the determination of the critical Reynolds number of Taylor–Couette flow with Newtonian fluids has been widely analyzed, and methodology has been established. However, this has not been established for non-Newtonian fluids. Therefore, the identification of the mode transition and determination of the critical Reynolds number led us to the useful design of devices in various industrial fields. In the experiment, the transition area of the Taylor-vortex flow as well as the wavy vortex flow with shear-thinning working fluids was first analyzed using optical measurement techniques, followed by the investigation of the flow transition mechanisms.

2. FLOW IN ROTATING CYLINDERS

Taylor–Couette flow has many flow regimes controlled by the Reynolds number, with surprisingly complex dynamics. In the most common conditions, the inner cylinder is rotating, and the outer cylinder is fixed.

The Reynolds number for the rotating cylinder system is defined below.

$$Re = \frac{\rho d r_i \Omega}{\mu_e} \qquad (1)$$

where ρ is the fluid density, μ_e is the effective
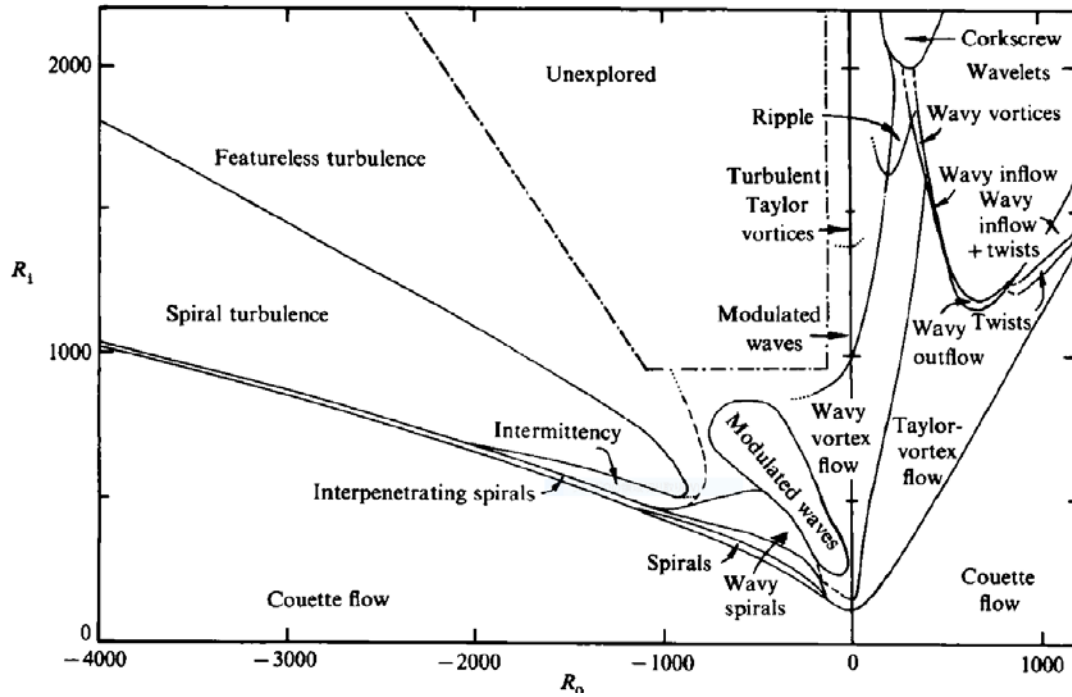
Fig.1 Flow regimes of two concentric rotating cylinder [13]

viscosity of the fluid, Ω is the rotational speed of the inner cylinder, d is the gap between the cylinders, and r_i is the inner cylinder radius. In the flow field, one of the differences between Newtonian and shear thinning flow is the velocity gradient near the nonslip wall. The shear stress acting on the fluid is given by the following model equation. For Newtonian fluids, the viscosity becomes constant, and the parameter n in the equation is equal to one.

$$\tau = \mu^* \left(\frac{du}{dy}\right)^n \qquad (0 < n < 1) \qquad (2)$$

where τ is the shear stress and μ^* is the reference viscosity. u and y are velocity and spatial coordinates, respectively. The y-axis is perpendicular to the main flow. The coefficient n is called the structural viscosity index of the power-law model. From the equation, the velocity gradient in the vicinity of the solid wall is increased with decreasing parameter n. That is a smaller n results in a higher shear thinning effect in fluids.

Andereck and Swinney [13] observed that the flow transitions between states were determined by *Ri* and *Ro* (inner- and outer-cylinder Reynolds numbers, respectively). Figure 1 shows the regimes observed in the flow between independently rotating concentric cylinders. Since the rotation speed of the outer cylinder is equal to zero in this research, flow regimes begin with the circular-Couette flow (CCF), Taylor-vortex flow (TVF), wavy vortex flow (WVF), and modulated wavy

vortex flow (MWF) and finally reach the turbulent Taylor vortex flow. CCF is laminar and axisymmetric under Reynolds numbers below the first critical Reynolds number, Re_{c1}. When the Reynolds number is increased beyond the critical value Re_{C1}, the flow becomes unstable, and a transition from CCF to TVF occurs. In the TVF regime, a series of steady toroidal rotating vortices are dominant in a cavity. Beyond the second critical Reynolds number, Re_{C2}, the series of vortices becomes unsteady and oscillates with a single frequency. This state corresponds to WVF. A further increase in the Reynolds number is associated with more transitions, which include MWF oscillation at two or more complicated frequencies, ultimately leading to turbulence.

The study of Taylor–Couette flow was mainly initiated by Taylor [14] for standard Newtonian fluids and has been the focus of considerable attention until now. The numerical predictions by Lockett et al. [15], Khali et al. [16], Alibenyahia et al. [11], and Ashrafi [9] reported that the shear thinning characteristics of the working fluid affect the mode transition of the flow and that the resultant critical Reynolds number becomes lower. By using a deterministic approach to analyze the nonlinear flow stability, the related results demonstrated that the dynamics of flow transition are completely different in Taylor–Couette flow with Newtonian working fluids and are caused by the shear thinning properties of the fluid. Cagney and Balabani [17] examined four fluids with different structural
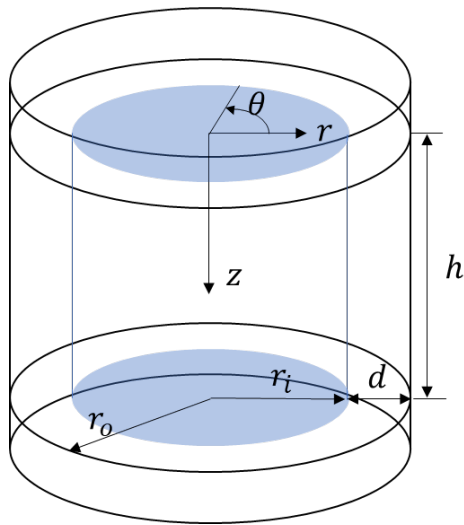
Fig.2 Experimental equipment and coordinates.

viscosity indices. Three of them exhibit shear thinning and viscoelasticity as well. They confirmed that shear thinning lowered the critical Reynolds numbers for TVF and WVF compared with those of Newtonian flow and calculated the amplitudes of inflow moving toward the inner cylinder and outflow moving toward the outer cylinder using the particle image velocity (PIV). They reported that the magnitude of vorticity, as well as that of the outflow, were both reduced in shear-thinning fluids relative to that of the Newtonian case. In the WVF of Newtonian fluids, the magnitude of inflow is lower than that at the outflow, but the magnitudes of inflow and outflow both tend to be significantly larger for shear-thinning fluids. They also indicated slow drifts in the axial positions of vortices and spatial variations in the wavy instability, which are not observed in Newtonian fluids. Most of the dynamics for shear thinning fluids of Taylor–Couette flow are still unclear, and a more detailed experimental investigation is desired. One of the previous studies

Fig.3 Schematic diagram of the concentric double cylinders and PIV measurement system. Laser sheet is parallel to the *r-z* plane in a cavity.

[17] obtained the critical Reynolds numbers of TVF and WVF for shear-thinning fluids. However, elucidation of the mechanism remains an issue for flow mode transition. This paper describes the identification of transition regimes using PIV with shear thinning working fluids and considers them.

3. EXPERIMENTS

The geometry of the experimental device used in the experiments is depicted in Fig.2. In the figure, the cylindrical coordinates r, θ, and z represent the radial, circumferential, and axial axes, respectively. The material of the cavity is transparent acrylic resin, and the water jacket is prepared around the outer cylinder to reduce the refraction effects of the light scattered from the small tracer particles in the fluid flow. Table 1 shows the representative dimensions of the experimental equipment. The inner cylinder is connected to the electrical motor via a belt. The rotation speed, which affects the Reynolds number, can be kept constant by the appropriate motor driver unit. In this study, the velocity distribution of the fluid flow was measured by the particle image velocimetry (PIV) technique.

A schematic diagram of the PIV measurement system is illustrated in Fig.3. A laser sheet was introduced into the vertical cross-section of the cavity. The tracer particles used in the PIV measurement were Dantec Dynamic, S-HGS silver-coated hollow glass spheres, in which the reflected light intensity from the tracer particle was enhanced by the metal coating of the spherical surface. The arithmetic means the diameter of the particles was approximately 10 μm, and the particle density was 0.68 g/cm^3. The frame rate of the image acquisition was 500 to 1000 fps depending on the particles' displacement between consecutive images, and the pixel dimensions of the CMOS sensor were 1280×768 pixels, which is varied by the maximum frame rate of the image acquisition. After confirming the steady state of the flow under each Reynolds number, 2000 to 4000 consecutive particle images were recorded in the memory of a PC, followed by cross-correlational velocity vector determination from the captured particle images.
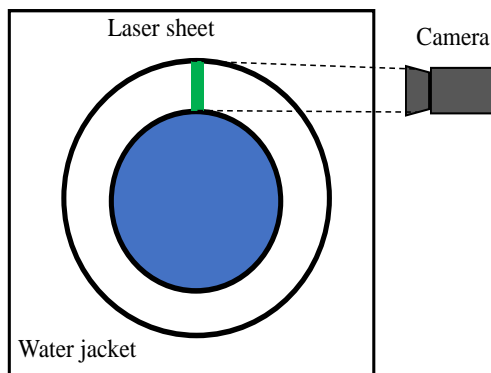
Table 1 Dimensions of the experimental rig.

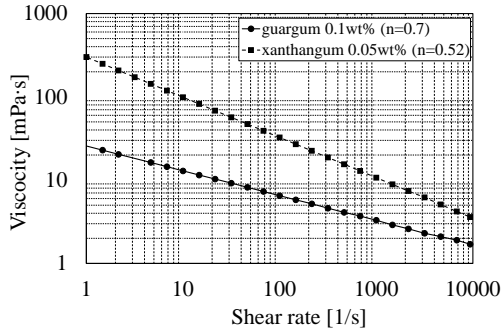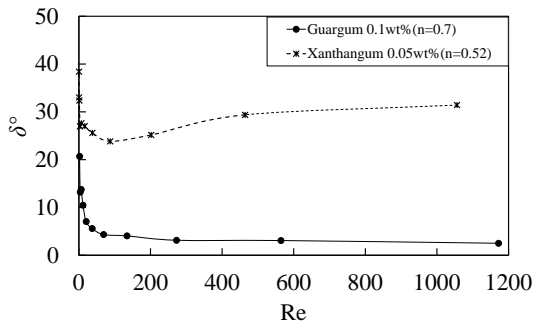| Parameter, units	Value
The radius of the inner cylinder, r_i [mm]	64.0
The radius of the outer cylinder, r_o [mm]	80.0
Height, h [mm]	96.0
The gap between cylinders, d [mm]	16.0
Radius ratio, $\eta = r_i / r_o$	0.8
The aspect ratio of the cavity, $\Gamma = h/d$	6.0

Fig.4 Rheological properties of the working fluid.

Fig.5 $\delta° = \tan^{-1} G''/G'$ vs. the Reynolds number. G'' is elastic modulus, and G' is the storage modulus.

With the Newtonian working fluid, the viscosity distribution is independent of the flow field, i.e., the viscosity is spatially and temporally homogeneous. However, with shear-thinning fluids, the velocity gradient at the bulk area in a cavity is higher, and the local effective viscosity is a function of the local shear rate. To reflect the spatial distribution of viscosity and to determine the effective Reynolds number, the effective viscosity is introduced by referring to Masuda et al. [18]. By this method, the effective shear rate is given by the following equation.

$$\dot{\gamma}_{eff} = k\Omega \qquad (3)$$

where k is the coefficient. The coefficient, k, is expressed by the following equation, which is determined by n and η, under the condition of $\eta \geq 0.7$. This can be effective because a wider gap has a larger viscosity ratio between the inner and outer walls than a narrow gap.

$$k(n, \eta) = 77.05n^{0.32}\eta^2 - 88.73n^{0.31}\eta + 26.85n^{0.21} \qquad (4)$$

The effective viscosity is shown using the Carreau model by the following equation.

Fig.6 Flow visualization by flake-shaped particles at the Re = 600 (top : n=0.7, bottom : n = 0.52)

$$\mu(\dot{\gamma}) = \mu_\infty + (\mu_0 - \mu_\infty)(1 + (\lambda_c\dot{\gamma})^2)^{\frac{n-1}{2}} \qquad (5)$$

where μ_0 is zero viscosity and μ_∞ is infinite viscosity. λ_c is the relaxation time. From the above results, the identification of the transition region is evaluated using the Reynolds number in Eq. (1).

4. RHEOLOGICAL PROPERTIES OF FLUIDS

To consider the shear thinning characteristics of fluid flow between rotating cylinders, two different working fluids were prepared that have different structural viscosity indices. One was a water solution of guar gum (GUAR) at 0.1 wt%, and the other was that of xanthan gum (XTG) at 0.05 wt%. The resultant viscosity indices were $n = 0.7$ and $n = 0.52$, respectively. Both working fluids were prepared by mixing the powders and distilled water with a blade stirrer at 700 rpm for 30 minutes. After the mixing procedure, the fluids were stored in the refrigerator for one day. The rheological properties of the fluids were first checked by a rotating rheometer. The measurement results are shown in Fig.4 and Fig.5. The important rheological

parameters in the experiments are shown in Table 2. The range of the shear rate magnitude in the following experiments was 10 to 150 s^{-1}.

Table 2 Fluid properties used in the experiment.

Fluid	n	μ_0 [10^{-3} Pa·s]	λ_c [s]
GUAR 0.1 wt%	0.7	51	0.55
XTG 0.05 wt%	0.52	820	0.76

5. FLOW VISUALIZATION

By using the working fluids shown in the previous section, the flow transition behavior in terms of the Reynolds number was first visualized by using flake-shaped visualization tracer particles, by which the local share direction can be qualitatively obtained. The Reynolds numbers varied from 0 to 650 for $n = 0.52$ liquid and from 0 to 850 for $n = 0.7$ liquid. Figure 6 shows examples of instantaneous flow visualization photographs. The Taylor vortices on the upper and lower end surfaces were slightly different in terms of vertical size due to the influence of the Ekman boundary layer. In contrast to the stretched aspect of vortices, convectional Newtonian fluids yield a series of toroidal square vortices, and each cell size is almost the same under the TVF and WVF modes [19].

If the cylinders are infinitely long, a series of infinite vortex trains are expected for Newtonian fluids, and a series of infinite irregular vortex trains are expected for non-Newtonian fluids. For the 0.1 wt% guar gum fluid with $n = 0.7$, the flow transition started with a simple circumferential Couette flow, followed by a series of steady toroidal vortices with a six-cell mode. In this stable stage, each cell geometry was almost the same when the Re number was below 90. Under the range of Re numbers from 90 to 850, the flow pattern entered the WVF mode, and toroidal cell fluctuations were observed. For 0.05 wt% xanthan gum fluid with $n = 0.52$, the flow pattern started with a simple circumferential Couette flow as well, and a series of steady toroidal vortices with four cell modes was observed. In this mode, each cell size was kept constant between Re = 0 and 65.

At Reynolds number beyond the critical Re number, the flow pattern changed to the WVF mode, in which the series of toroidal vortices were significantly different from those of the Newtonian working fluid. The upper and lower vortices became vertically enlarged, and the degree of deformation was affected by the Reynolds number. In contrast, the vortex at the center of the cavity was squeezed at the WVF. Fig.7 summarizes the relationship between the Reynolds number and vortex dimension compared with those of working fluid with Newtonian characteristics. The vertical
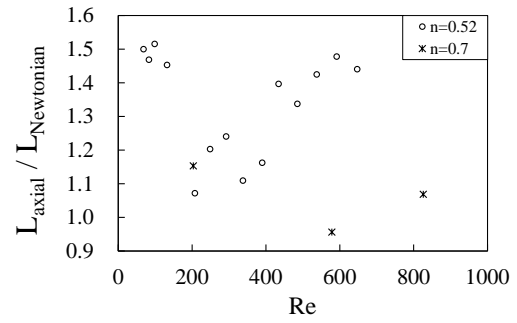

Fig.7 The ratio of the axial lengths of the vortex relative to that of a Newtonian fluid in terms of the Reynolds number.

axis in the figure denotes the nondimensional axial lengths of the vortex about the vortex size with Newtonian fluid. With Z_1 and Z_2 defined as the center positions of the first and second vortices from the top end wall, the relationship between both vortex positions in terms of the Reynolds number is depicted in Fig.8. In contrast to the convectional Taylor vortex flow with a Newtonian working fluid, both central vortex heights are drastically decreased, and the size ratio between neighboring vortices is remarkably varied as the Reynolds number increases.
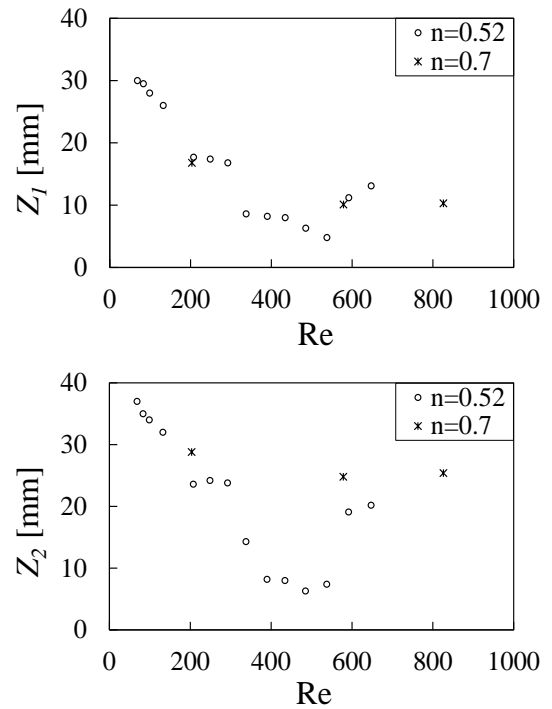
6. CRITICAL REYNOLDS NUMBERS

Fig.8 Vertical position of the vortex, Z_1, Z_2, as a function of the Reynolds number.
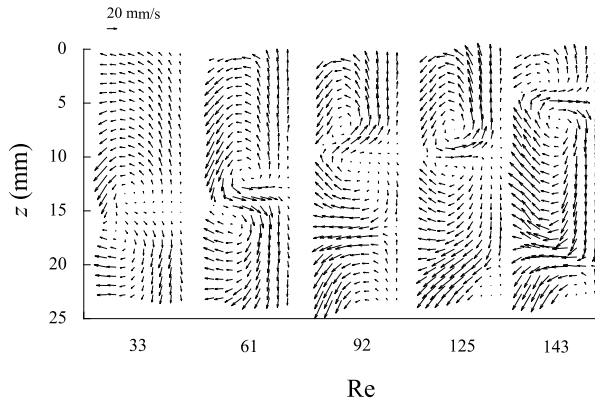
Fig.9 Instantaneous velocity vector map at various Reynolds number measured by particle image velocimetry (PIV).

Velocity distributions were obtained using the PIV technique from consecutive particle images acquired by a digital high-speed camera. The critical Reynolds numbers between the TVF and WVF regimes were determined by the fluctuation of the velocity profile as well as the power spectrum of the velocity vectors at the bulk area. Letting Re_{C1} and Re_{C2} denote the critical Reynolds numbers for TVF and WVF, respectively. Re_{C1} is determined by the velocity distribution when steady toroidal vortices are observed. The mean velocity distributions are shown in Fig.9. Re_{C2} is determined from the spectrum analysis result by acquiring the velocity time series data of each window from the velocity distribution and spatial averaging of the power spectrum. In the WVF regime, the spectrum exhibited a single peak frequency that correlated with wavy motion, and the entire Taylor vortex oscillated at a particular frequency. The measured relation between the peak frequency and Reynolds number is shown in Fig.10. From the above process, both critical Reynolds numbers are summarized in Tbl. 3 compared with those of the Newtonian case from reference [19].

Table 3 Summary of resultant Re_{C1} and Re_{C2} for both working fluids.

n	Re_{C1}	Re_{C2}	f (WVF) [Hz]
1	95	1330	~1
0.7	92.6	608.7	3.67
0.52	65	93.1	0.68

In the analysis of the measurement results of velocity vector distributions, significantly different velocity fields were observed due to the shear thinning effects of working fluids, unlike the case of Newtonian fluids. The geometrical shape, such
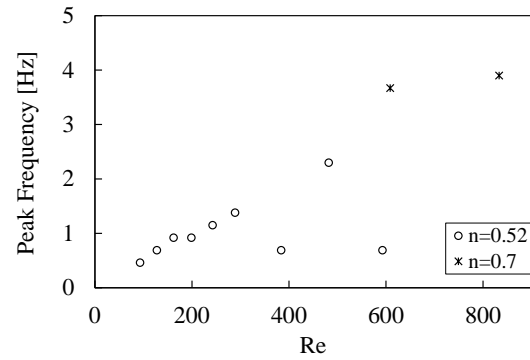

Fig.10 Peak frequency of fluid flow modulation in terms of Reynolds number as well as the power law index, n

as the aspect ratio of the vortices, was not identical to that of the Newtonian fluid. With the working fluid of $n = 0.52$, a characteristic four-cell mode appeared, and the size of upper and lower edge vortex cells was significantly stretched compared with those of the central cells. As the Reynolds number increased, as shown in Fig.7, the size of the vortex increased in the axial direction, and the position of the vortex gradually moved along the axial direction in the WVF regime. Table 3 summarizes the critical Reynolds numbers as a function of the power-law index n. The result showed that every critical Reynolds number was much lower than the critical Reynolds number for a Newtonian fluid. Similar to what Cagney and Balabani [17] reported, the present results lead us to conclude that the critical Reynolds number between TVF and WVF with shear thinning fluids is quite different from that of Newtonian fluids. One possible difference is the definition of the Reynolds number. They prepared four kinds of working fluids, one of which was a Newtonian fluid and three of which had different viscosity indices. They confirmed that the shear-thinning characteristics of the working fluid make the critical Reynolds number lower than that of the Newtonian case, but there are no large differences. In our experiment, the critical Reynolds numbers for TVF were not varied. Shear-thinning effects, however, make the critical Reynolds number for WVF lower than that of the Newtonian fluid. Since the shear-thinning effect significantly increases the viscosity gradient between the vicinity of the wall surface and the main flow, the local velocity gradient in the circumferential direction is exponential, as shown in Eq. (2). Consequently, the pair of vortices can easily oscillate in the vicinity of the solid wall and pulsate when the wall binding force is decreased due to the larger velocity gradient at the boundary layer near the rotating cylinder.

7. CONCLUSION

In this study, the fluid flow behavior between double concentric cylinders was experimentally investigated using particle image velocimetry. Two different types of shear-thinning fluids were used and compared. By using a rotating cylinder with an electrically controlled motor, the Reynolds number was varied through the CCF, TVF and WVF regimes. The flow dynamics were examined using the measured velocity vector field in the vertical cross-section. The time-averaged velocity field indicated that the shear thinning effects of the working fluid induced the vertical elongation of the edge vortex and that the position of the vortex center was vertically displaced as the Reynolds number increased under the WVF regime. The critical Reynolds numbers for the transition to both TVF and WVF were affected by the shear-thinning characteristics of the working fluid. The lower index n enhanced the flow mode transition in contrast to that of Newtonian working fluids. In particular, the critical Reynolds number in the WVF regime was significantly decreased with the lower index n due to the reduced wall binding force in the vicinity of the rotating wall.

8. REFERENCES

[1] Holeschovsky U.B. and Cooney C.L., Quantitative description of ultrafiltration in a rotating filtration device, AIChE J., Vol. 37, 1991, pp. 1219-1226.

[2] Hill E.K., Krebs B., Goodall D.G., Howlett G. J. and Dunstan D.E., Shear flow induces amyloid fibril formation, Biomacromolecules, Vol. 7, 2006, pp. 10-13.

[3] Ameer G.A., Grovender E.A., Obradovic B., Cooney C.L. and Langer R., RTD analysis of a novel Taylor-Couette flow device for blood detoxification, AIChE J., Vol. 45, 1999, pp. 633-638.

[4] Vedantam S. and Joshi J.B., Annular centrifugal contactors-A review, Chem. Eng. Res. Des., Vol. 84, 2006, pp. 522-542.

[5] Haut B., Ben Amor H., Coulon L., Jacquet A. and Halloin A., Hydrodynamics and mass transfer in a Couette-Taylor bioreactor for the culture of animal cells, Chem. Eng. Sci., Vol. 58, 2003, pp. 777-784.

[6] Kataoka K., Ohmura N., Kouzu M., Simamura Y. and Okubo M., Emulsion Polymerization of Styrene in a Continuous Taylor Vortex Flow Reactor, Chem. Eng. Sci., Vol. 50, 1995, pp. 1409-1416.

[7] Jung, T., Kim W.S. and Choi C.K., Effect of Monovalent Salts on Morphology of Calcium Carbonate Crystallized in Couette-Taylor Reactor, Cryst. Res. Technol., Vol. 40, 2005, pp. 586-592.

[8] Dutta P.K. and Ray A.K., Experimental Investigation of Taylor Vortex, Photocatalytic Reactor for Water Purication, Chem. Eng. Sci., Vol. 59, 2004, pp. 5249-5259.

[9] Ashrafi N., Stability analysis of shear-thinning flow between rotating cylinders, Appl. Math. Modell. Vol. 35, 2011, pp. 4407-4423.

[10] Coronado-Matutti O., Souza Mendes P.R. and Carvalho M.S., Instability of inelastic shear-thinning liquids in a Couette flow between concentric cylinders, J. Fluids Eng. Vol. 126, 2004, pp. 385-390.

[11] Alibenyahia B., Lemaitre C., Nouar C. and Ait-Messaoudene N., Revisiting the stability of circular Couette flow of shear-thinning fluids, J. Non-Newtonian Fluid Mech., 2012, Vol. 183-184, pp. 37-51.

[12] Escudier M.P., Gouldson I.W., and Jones D.M., Taylor vortices in Newtonian and shear-thinning liquids, Proc. R. Soc. London, Ser. A 449, 1995, pp. 155-175.

[13] David A.C., Liu S.S. and Harry L.S., Flow regimes in a circular Couette system with independently rotating cylinders, J. Fluid Mech., Vol. 164, 1986, pp. 155-183.

[14] Taylor G.I, Stability of a viscous liquid contained between two rotating cylinders, Phil. Trans. R. Soc. Lond. Vol. A 223, 1923, pp. 289-343.

[15] Lockett T.J., Richardson S.M. and Worraker W.J., The stability of inelastic non-Newtonian fluids in Couette flow between concentric cylinders: A finite-element study, J. Non-Newtonian Fluid Mech. Vol. 43, 1992, pp. 165-177.

[16] Khali S., Nebbali R., and Bouhadef K., Numerical investigation of non-Newtonian fluids flow between two rotating cylinders using the lattice-Boltzmann method, Int. Scholarly Sci. Res. Innovation, Vol. 7, 2013, pp. 1999-2005.

[17] Cagney N. and Balabani S., Taylor-Couette flow of shear-thinning fluids, Phys. Fluids, Vol. 31, 2019, 053102.

[18] Masuda H., Horie T., Hubacz R., Ohta M. and Ohmura N., Prediction of onset of Taylor-Couette instability for shear-thinning fluids, Rheologica Acta, Vol. 56, 2017, pp. 73-84.

[19] Noguchi Y., Saito T. and Kawaguchi T., Flow Structure Analysis of Taylor-Couette Flow in Low Aspect Ratio Cell Department of Mechanical Engineering, MS-thesis of Tokyo Institute of Technology, 2019.